frontiers | Frontiers in Physics

TYPE Original Research
PUBLISHED 24 April 2024
DOI 10.3389/fphy.2024.1385314

OPEN ACCESS

EDITED BY
Javier Resta López,
University of Valencia, Spain

REVIEWED BY
John Wesley Lewellen,
Los Alamos National Laboratory (DOE),
United States
Mikhail Krasilnikov,
Helmholtz Association of German Research
Centres (HZ), Germany

*CORRESPONDENCE
Amir Weinberg,
amirwe@tauex.tau.ac.il
Avraham Gover,
gover@eng.tau.ac.il

RECEIVED 12 February 2024
ACCEPTED 02 April 2024
PUBLISHED 24 April 2024

CITATION
Weinberg A, Gover A, Nause A, Friedman A, Ianconescu R, Fisher A, Musumeci P, Fukasawa A and Rosenzweig J (2024), Theory and design consideration of a THz superradiant waveguide FEL.
Front. Phys. 12:1385314.
doi: 10.3389/fphy.2024.1385314

Theory and design consideration of a THz superradiant waveguide FEL

Amir Weinberg[1]*, Avraham Gover[1]*, Ariel Nause[2], Aharon Friedman[2], Reuven Ianconescu[3], Andrew Fisher[4], Pietro Musumeci[4], Atsushi Fukasawa[4] and James Rosenzweig[4]

[1]School of Electrical Engineering—Physical Electronics, Center of Light-Matter Interaction, Tel Aviv University, Tel Aviv, Israel, [2]The Schlesinger Center for Compact Accelerators and Radiation Sources, Ariel University, Ariel, Israel, [3]Shenkar College, Ramat Gan, Israel, [4]Department of Physics and Astronomy, University of California, Los Angles, United States

We present theoretical analysis and design considerations of a THz superradiant FEL. We derive analytical expressions for the spectral parameter of THz radiation, emitted superradiantly in a rectangular waveguide using a Longitudinal Section Magnetic mode expansion. The results compare well with numerical simulations using UCLA GPTFEL code. GPT simulations of the accelerator e-beam transport show that the chirp provided by a hybrid photocathode RF gun, can produce tight bunching at the undulator site below σ = 100fs. This enables intense superradiant emission up to 3THz, limited by the beam bunching factor. Phase-space analysis of the beam transport indicates that keeping the beam bunching parameter small enough for higher THz frequency operation is limited by the energy spread of the beam in the gun.

KEYWORDS

FEL, superradiance, waveguide LSM modes, GPTFEL, THz, hybrid photocathode gun, coherent undulator radiation, bunched beam

1 Introduction

Bunched beam superradiance is the coherent spontaneous radiation emission of a bunch of electrons, taking place when the bunch duration σ_t is shorter than the optical period $(2\pi/\omega)$ of the radiation [1]. This process is analogous to the superradiance of an ensemble of dipole-excited molecules proposed first by Dicke [2]. When this condition is satisfied, the radiation emission of the bunch is proportional to the number of electrons in the bunch, squared (N^2). This is a substantial enhancement of many orders of magnitude in comparison to spontaneous emission by a long duration beam that is proportional to the number of electrons in the bunch (N).

Here we extend earlier theory of bunched-beam superradiance [1, 3], and apply it to evaluate and optimize the spectrum and energy of a compact THz FEL shown schematically in Figure 1. This experimental setup is based on the design of the Israeli hybrid 6 MeV photocathode RF gun [4]. A picosecond electron bunch emitted from the cathode is accelerated and chirped within the short (0.6 m) hybrid accelerator, and then compressed through free drift compression, velocity bunching (ballistic compression) [5–7] along a 3.4 m beamline to $\sigma_t \approx 70\,fs$, as predicted by GPT simulations including space charge effects [8, 9] (see the lower panel of Figure 1). The superradiant THz pulse is generated in an over-moded rectangular waveguide placed within a short planar magnetic undulator (0.8 m).

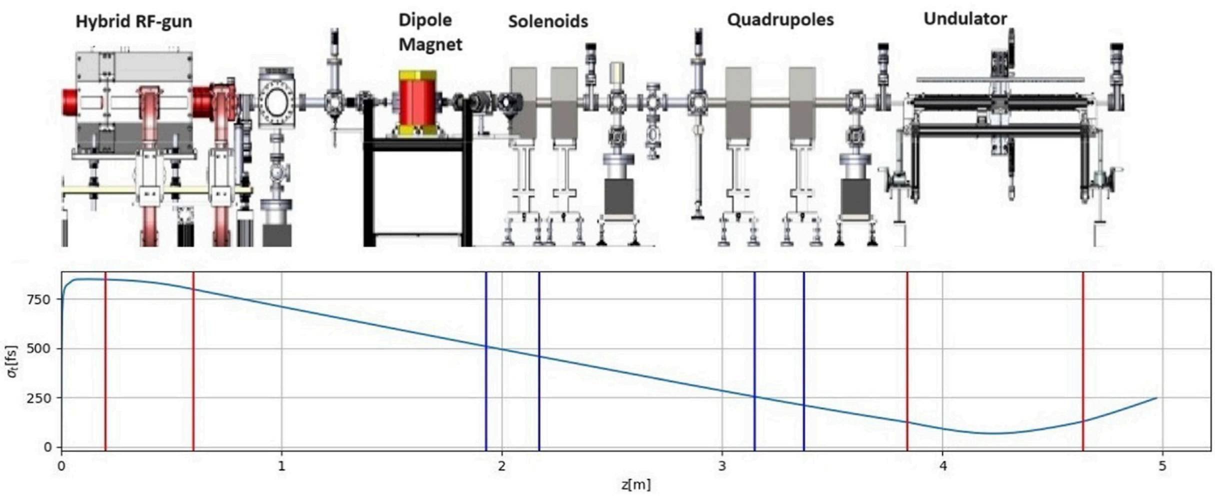

FIGURE 1
Top: A sketch of the ORGAD (optically excited RF GUN accelerator device) accelerator. Bottom: bunch duration evolution along the ORGAD FEL beamline.

2 Emission energy and spectrum of a superradiant waveguide FEL

We present here the formulation for calculating the spectral energy and total emission energy of superradiant waveguide FEL. Using the formulation of [1], the spectral energy per emitted radiation mode q in the case of a perfectly bunched electron beam (zero length bunch—farther down we generalize to a finite length bunch) is:

$$\left(\frac{dW_q}{d\omega}\right)_{SP-SR} = \frac{N^2e^2Z_q}{16\,\pi}\left(\frac{\bar{a}_w}{\beta_z\gamma}\right)^2\frac{L_w^2}{A_{eff,q}}sinc^2\left(\frac{\theta L_w}{2}\right) \tag{1}$$

and its integrated energy is:

$$W_q = \frac{N^2e^2Z_q}{16\,\pi}\left(\frac{\bar{a}_w}{\beta_z\gamma}\right)^2\frac{L_w^2}{A_{eff,q}}\frac{\omega_{0,q}}{N_w} \tag{2}$$

These equations are valid for any complete orthogonal mode expansion in free space or in a waveguide. In the case of conventional free space FEL $Z_q = \sqrt{\mu_0/\varepsilon_0}$, in a waveguide it is the waveguide mode impedance. The effective area of the mode is $A_{eff,q} = \frac{\iint |E_{q\perp}(x,y)|^2dxdy}{|E_{qx}(x_0,y_0)|^2}$, where ($x_0$, y_0) are the transverse coordinates of the beam propagation axis. In these equations N is the number of particles, c is the speed of light, e is the electron charge, γ is the beam energy Lorentz factor, the rms average of the undulator parameter $a_w = \frac{eB_w}{mck_w}$ is $\bar{a}_w$(m is the electron mass, B_w is magnetic field amplitude). β_z is the longitudinal velocity of the beam inside the undulator, L_w is the undulator length, N_w is the number of undulator periods. The FEL detuning parameter is defined by:

$$\theta = \frac{\omega}{v_z} - k_{z,q} - k_w \tag{3}$$

Where $k_w = \frac{2\pi}{\lambda_w}$ is the periodic undulator wavenumber, $k_{z,q} = \sqrt{\left(\frac{\omega}{c}\right)^2 - k_{\perp,q}^2}$ is the longitudinal wavenumber of mode q, where $k_{\perp,q}$ is the transverse wave number of the mode.

The spectral energy of the radiation mode (Eq. (1)) depends on frequency through the tunning parameter $\theta_q(\omega)$. The center frequency of the spectral radiation (1) corresponds to $\theta_q(\omega) = 0$. In a waveguide, this equation has two solutions [10]. We refer here to the higher frequency (+) solution only:

$$\omega_{0,q} = \gamma_z^2\beta_z ck_w\left(1 \pm \sqrt{\left(\beta_z^2 - \left(\frac{k_{\perp,q}}{\gamma_z k_w}\right)^2\right)}\right) \tag{4}$$

The formulation so far is valid for any waveguide mode expansion. We consider an FEL configuration based on a rectangular waveguide and planar undulator polarized in the y direction (see Figure 2). For this configuration we find it most productive to use a waveguide expansion set of LSM (Longitudinal Section Magnetic) modes [11]. This is an alternative to the conventional TE TM mode expansion. The LSE^x modes (characterized by $E_x = 0$) and LSM^x modes (characterized by $H_x = 0$), are a complete set of orthogonal modes, equivalent to the {TE, TM} mode expansion. In a planar undulator configuration, shown in Figure 2, the wiggling of the electron beam, and thus the excitation current, are in the x dimension. Therefore, in the {LSE^x, LSM^x} expansion, we can eliminate the LSE^x modes, since they cannot be excited by the beam current, and thus we manage to describe the radiation field in terms of half the number of modes of the degenerate {TE, TM} mode expansion. We therefore calculate only the excitation of the LSM^x modes given by [11]:

$$\begin{aligned}
E_z &= \sin(k_x x)\sin(k_y y)\\
E_x &= \frac{k_y^2 + k_z^2}{ik_x k_z}\cos(k_x x)\sin(k_y y)\\
E_y &= -\frac{k_y}{ik_z}\sin(k_x x)\cos(k_y y)\\
H_z &= -\frac{\omega\epsilon k_y}{\beta k_x}\cos(k_x x)\cos(k_y y)\\
H_y &= -\frac{i\omega\epsilon}{k_x}\cos(k_x x)\sin(k_y y)
\end{aligned} \tag{5}$$

10.3389/fphy.2024.1385314

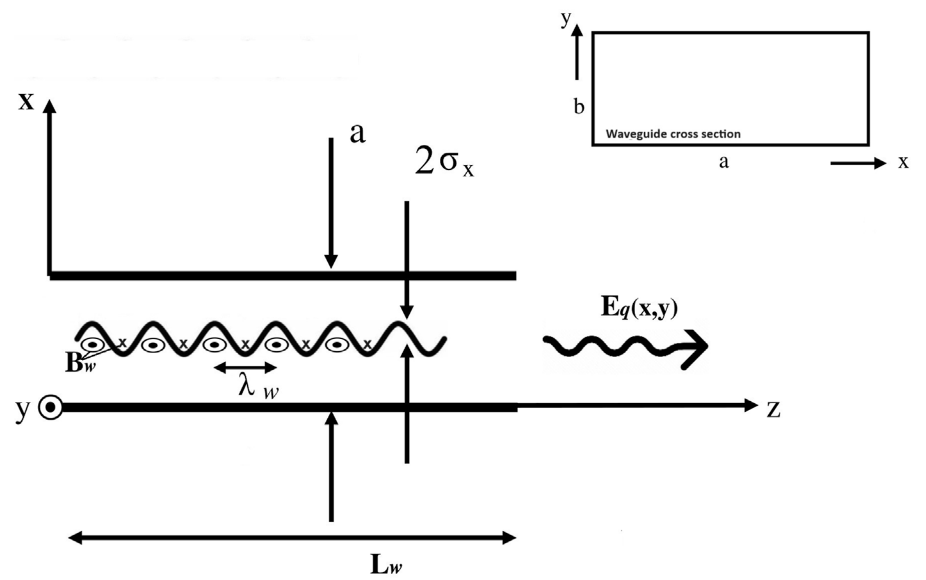

FIGURE 2
Rectangular waveguide coordinates and dimensions, (a) waveguide width, (b) waveguide height, L_w—undulator length.

$$
\begin{aligned}
k_{z,mn} &= \sqrt{\left(\frac{\omega}{c}\right)^2 - k_{\perp,mn}^2} \\
k_{\perp,mn} &= \sqrt{k_{yn}^2 + k_{xm}^2} \\
k_{xm} &= \frac{m\pi}{a} \quad m = 0, 1, 2... \\
k_{yn} &= \frac{n\pi}{b} \quad n = 0, 1, 2... \\
Z_{LSM} &= Z_0 \frac{k_y^2 + k_z^2}{kk_z}
\end{aligned}
\tag{6}
$$

ω is the frequency of the radiation mode, ε is the permittivity inside the waveguide. $Z_0 = \sqrt{\mu_0/\varepsilon_0}$ is the impedance of free space $k = \omega/c$, $k_{z,mn}$ (ω) is the longitudinal wavenumber of the mode (also the dispersion relation of the mode). For an axi-symmetric electron beam propagating along the waveguide axis, we can refer to the symmetry of the modes and eliminate all the modes that are null on axis. Therefore, only the modes m = 0,2,4. . . n = 1,3,5. . .that have finite amplitude $E_x\left(\frac{a}{2}, \frac{b}{2}\right) \neq 0$ can be excited.

Substituting the fields of the excitable modes (5) in the excitation Equation 1, we calculated the spectral energy of the emitted radiation for the first lower 9 modes of the waveguide. For the designed example parameters, listed in Table 1, the radiation energies of these modes are listed in the third row of Table 2.

In practice the beam transverse dimension and its longitudinal bunching are not ideal. We considered here also the case of a beam of finite transverse and longitudinal dimensions assuming gaussian distribution. The effects of the transverse distribution of the beam can be taken into account by convolving Eq. (1) with the normalized transverse distribution of the beam profile, which gets modified because of the (x_0, y_0) dependances of the effective mode area $A_{eff,q}$.

TABLE 1 Parameters of the ORGAD superradiant FEL.

Parameter	Units	
waveguide width a	mm	12.954
Waveguide height b	mm	6.477
Undulator period λ_w	mm	20
Number of periods N_w		40
Undulator interaction length L_w	m	0.8
Undulator wavenumber k_w	1/m	314.16
Undulator magnetic field amplitude B_w	T	0.49
Undulator parameter a_w		0.9151
One period rms average of a_w $\bar{a}_w$		0.6470
Beam energy Lorenz factor γ		13.1
$\gamma_z = \frac{\gamma}{\sqrt{1+\bar{a}_w^2}}$		11

This was calculated in Supplementary Appendix B for the LSM^x modes. In Figure 3 we show the spectrum of the first 9 modes of the waveguide computed from Eq. (1) with the parameters of Table 1 including the effect of transverse beam dimensions for $\sigma\perp = 0.5$ [mm]. The bunch is considered to be ideally bunched in the longitudinal dimension ($\sigma\_t = 0$). In the fourth row of Table 2 we show the reduced emission energy of the excited modes assuming a transverse beam profile of standard deviation $\sigma_\perp = 0.5\,[mm]$. The emission energy is reduced relative to the ideally narrow beam $\sigma_\perp = 0$ given in the third line.

The total emitted superradiant energy and spectral energy of the modes would be reduced also by the finite longitudinal

TABLE 2 Emitted Energy W[nJ] computed from Eq. 2. The mode indices (m,n) (Eq. 6) correspond to the mode numbers in the wide (horizontal) x dimension and the height (vertical) y dimension of the rectangular waveguide respectably (see Figure 2). The third row corresponds to an ideal case of a delta function transverse beam profile. The fourth row—corresponds to a Gaussian transverse beam profile. In either case the bunch is ideally narrow in the longitudinal dimension.

m,n	0,1	0,3	0,5	2,1	2,3	2,5	4,1	4,3	4,5
f [THz]	3.5	3.45	2.98	3.48	3.33	2.96	3.43	3.26	2.88
$\sigma_{\perp} = 0$	63.362	60.548	53.857	126.042	120.346	106.730	123.952	118.037	103.637
$\sigma_{\perp} = 0.5[mm]$	59.846	40.778	28.351	112.443	76.553	53.067	95.104	64.577	44.318

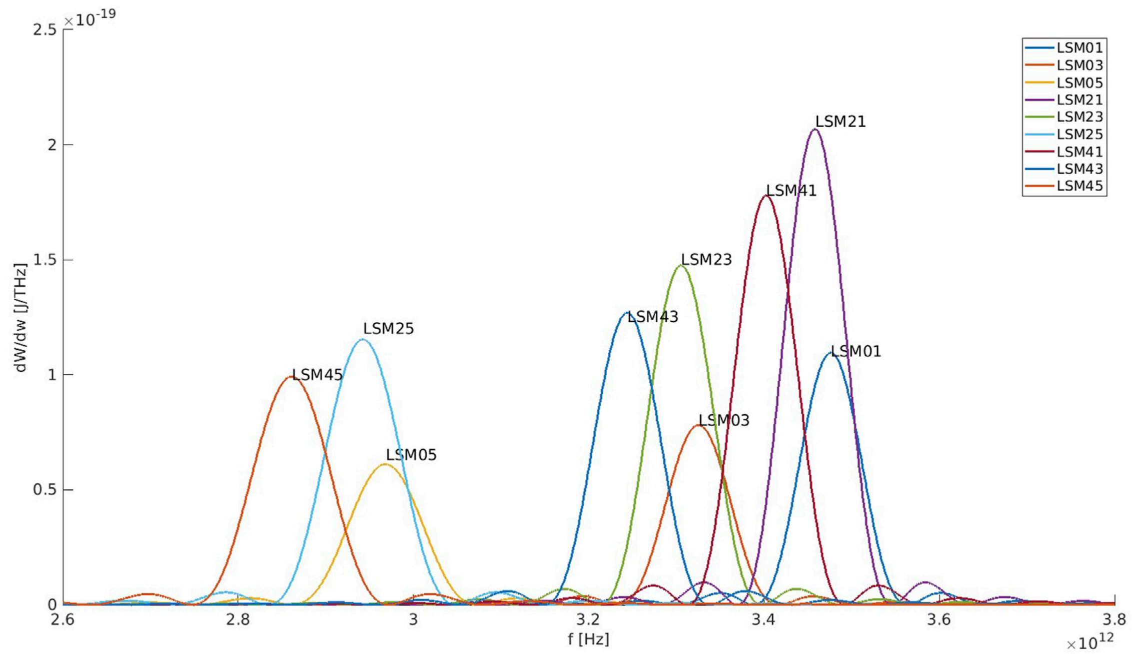

FIGURE 3
Spectral Energy of the first 9 excitable LSM modes for E = 6.2Mev, computed from Eq. 1 using the parameters of Table 1, The beam width and time duration are $\sigma_{x,y} = 0.5mm$ and $\sigma_t = 0$.

dimension of the beam. This is a result of destructive interference between the radiation wave packets emitted by distributed electrons when the short bunch condition is not satisfied. The spectral energy and total superradiant radiant energy are reduced by a bunching factor relative to the ideal zero-length bunch (eq. 1,2). For a bunch longitudinal profile represented by a Gaussian distribution of standard deviation σ_t emitting radiation at frequency f, the bunching factor is given by [1]:

$$\left|M_b(f)\right|^2 = e^{-(2\pi f\sigma_t)^2} \tag{7}$$

and the mode energy is:

$$W_{mn}(\sigma_t) = W_{mm}(\sigma_t = 0)|M_b|^2. \tag{8}$$

The bunching factor Eq. 7 is plotted in Figure 4 as a function of the emission frequency for various values of σ_t. Clearly, the drop of the bunching parameter at high frequencies determines the upper frequency limit of the superradiant source. The figure indicates that for a bunch of standard deviation 70 fs, the superradiant Terahertz FEL is limited to operation below f = 3 THz.

3 Numerical computation of superradiance

We compare the above analytical calculation results for the superradiant energy emission with numerical computations based on the UCLA GPTFEL code [12, 13] for a rectangular waveguide model. We performed the computations for the parameters of the ORGAD FEL configuration (Table 1). The comparison is made for the fundamental mode of the rectangular waveguide TE01 which is identical with the LSM01 mode used in the analytical calculation. Figure 5 displays the numerically simulated spectral energy of the mode TE01. The frequency spectrum in this model is presented in turns of longitudinal modes [12], and the beam at the entrance to the undulator is modeled in terms of a gaussian distribution. The spectral energy distribution computed by the numerical code is in good agreement with the corresponding curve of mode LSM01.

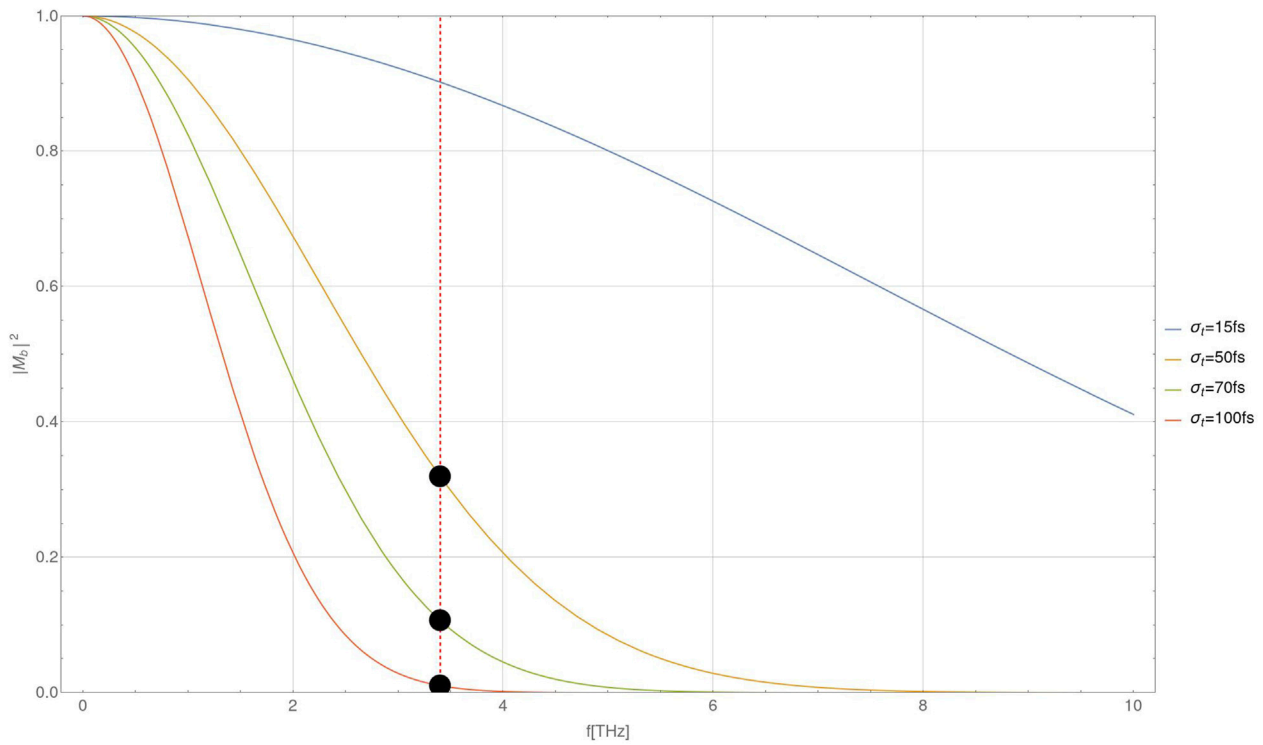

FIGURE 4
Bunching factor plotted as a function of frequency for different bunch durations σ_t.

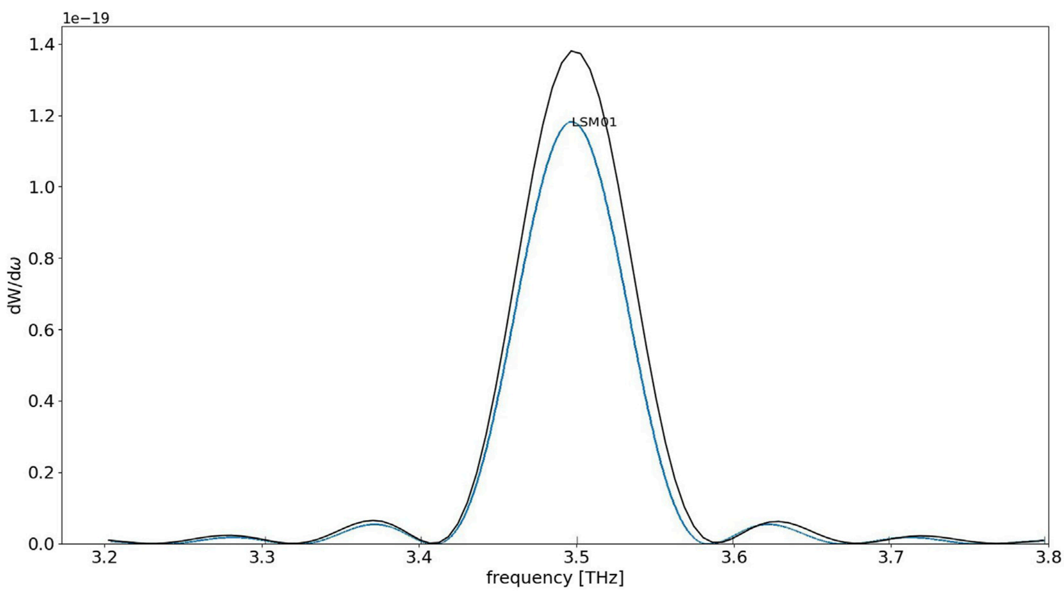

FIGURE 5
Simulated spectral energy of the LSM01 mode computed with UCLA GPTFEL for a nearly ideal short and narrow bunch of length σ_z = 5um (bunch duration σ_t = 16 fs), bunch transverse size $\sigma_\perp = 0.1mm$ (black curve) with no space-charge effects. For comparison, the spectral distribution emitted into the same mode by an ideal beam calculated from the analytical expression (Eq. 1), is overlayed (blue curve).

In Table 3 we compare the analytically calculated emission energy of the fundamental mode energy to the numerical simulation results for different values of the standard deviation of the beam bunch distribution σ_t. The calculated bunching factor (Eq. 7) and reduced emission energy (Eq. (8)) are listed in the third and fourth columns of Table 3. The numerically computed results, listed in the fifth column, are about 50%

TABLE 3 Comparison between analytical calculation and GPTFEL code computation of mode LSM01 (TE01).

Standard deviation of the bunch σ_t (σ_z)	Analyticalexpression $W(\sigma_{t=}0)$ (nJ)	Bunching factor $\lvert M_b\rvert^2$	Reduced mode energy $W(\sigma_t)$ (nJ)	GPT (nJ)
16 fs (5um)	63.4	0.89	56.4	83.4
33fs (10um)	63.4	0.6	38	58
50fs (15um)	63.4	0.32	20	30
66fs (20um)	63.4	0.131	8.317	12

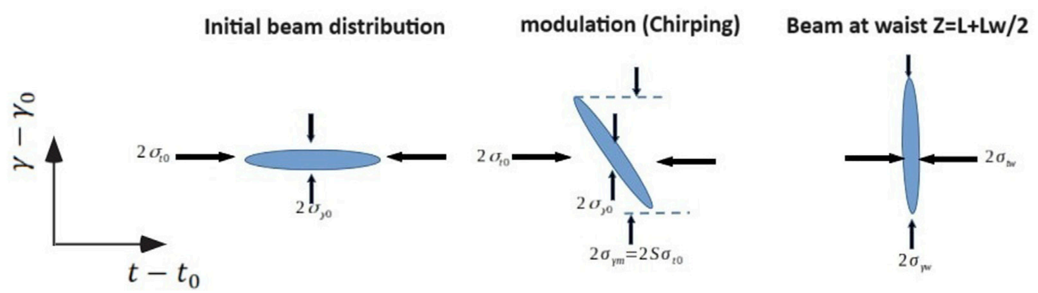

FIGURE 6
The evolution in $(\gamma - \boldsymbol{t})$ phase-space of a Gaussian bunch depicting modulation (chirping) of the beam and free space drift compression to a minimal longitudinal waist.

higher. They also indicate diminishing of the emission energy of the fundamental mode (centered at f = 3.4 THz) for $\sigma_t \approx 70\ fS$.

4 Phase space (γ-t) dynamics of beam compression

Since the high frequency operation of the superradiant terahertz source is limited by the size (duration) of the electron beam bunch within the length of the undulator, it is important to control the free drift self-compression of the beam from the gun to the undulator and attempt to minimize the bunch duration nearly at the center of the undulator. In Figure 6 we show the evolution in phase space of a Gaussian beam starting from the buncher (modulator) section of the gun, right after full acceleration, and then going through free drift transport up to the undulator. In our linear beam transport model, the phase-space area of the beam is conserved under linear transport transformations.

We model the initial distribution in γ-t phase-space of the accelerated beam (before bunching) in terms of a Gaussian function:

$$f_i(\gamma,t) = \frac{1}{2\pi\sigma_{t0}\sigma_{\gamma0}} e^{\frac{-(t-t_0)^2}{2\sigma_{t0}^2} + \frac{-(\gamma-\gamma_0)^2}{2\sigma_{\gamma0}^2}} = \frac{1}{2\pi\sigma_{t0}\sigma_{\gamma0}} e^{-\phi(\gamma,t)} \tag{9}$$

σ_{t0} is the beam standard deviation duration, at the entrance of the gun. $\sigma_{\gamma0}$ is the intrinsic (uncorrelated) energy spread (standard deviation) in the gun. As shown in Figure 6 the beam is chirped in the modulation section of the gun at a rate $S = \Delta\gamma/\Delta t$. Following this step, the beam is compressed through free space drift and passage through the undulator. The compression is characterized by the longitudinal dispersion factor (compaction parameter) R_{56}. After the modulation transformation (chirping in the gun):

$$\gamma - \gamma_0 \rightarrow \Delta\gamma + S\Delta t \tag{10}$$

$$\phi(\gamma,t) = \frac{(t-t_0)^2}{2\sigma_{t0}^2} + \frac{(\Delta\gamma + S\Delta t)^2}{2\sigma_{\gamma0}^2} \tag{11}$$

We Consider beam transport from the accelerator to the center of the undulator. In a linear phase-space dynamics model the beam phase-space distribution stretches in the time dimension according to

$$t - t_0 \rightarrow \Delta t + \frac{R_{56}}{c}\frac{\Delta\gamma}{\gamma_0} \tag{12}$$

The energy dispersion compaction parameter R_{56} is the result of free drift along a distance L from the gun to the undulator entrance and a subsequent drift within periodic magnetic field along half the length of the undulator:

$$R_{56}\left(La\frac{L_w}{2}\right) = \frac{1}{\gamma_0^2}\left[La\int_0^{\frac{L_w}{2}} a_\perp^2(z')dz'\right] \qquad a_\perp(z') = \mathrm{e/mc}\int_0^z B_\perp(z')dz' \tag{13}$$

where B⊥ is the undulator magnetic field. Substituting Eq. (12) in Eq. (11) we obtain:

$$\phi(L,\gamma,t) = \frac{\left(\Delta t + \frac{R_{56}}{c}\frac{\Delta\gamma}{\gamma_0}\right)^2}{2\sigma_{t0}^2} + \frac{\left(\Delta\gamma + S\left(\Delta t + \frac{R_{56}}{c}\frac{\Delta\gamma}{\gamma_0}\right)\right)^2}{2\sigma_{\gamma0}^2} \tag{14}$$

We receive an oblique ellipse contour:

$$\phi(L,\gamma,t) = \left[\frac{1}{2\sigma_{t0}^2} + \frac{S^2}{2\sigma_{\gamma 0}^2}\right](\Delta t)^2 + \left[\frac{1}{2\sigma_{\gamma 0}^2} + \frac{R_{56}^2}{2c^2\gamma_0^2\sigma_{t0}^2} + \frac{S^2R_{56}^2}{2c^2\gamma_0^2\sigma_{\gamma 0}^2} - \frac{R_{56}|S|}{c\gamma_0\sigma_{\gamma 0}^2}\right](\Delta\gamma)^2 + \left[\frac{R_{56}}{c\gamma_0\sigma_{t0}^2} - \frac{|S|}{\sigma_{\gamma 0}^2} + \frac{R_{56}S^2}{c\gamma_0\sigma_{\gamma 0}^2}\right](\Delta t\Delta\gamma) \tag{15}$$

Requiring attainment of a minimal duration bunch at the center of the undulator, we observe that this happens when the ellipse, keeping constant area, becomes erect. This corresponds to a requirement that the mixed term in Eq. 15 nulls. This corresponds to a condition for R_{56}:

$$R_{56} = \frac{c\gamma_0\sigma_{t0}^2 S}{S^2\sigma_{t0}^2 + \sigma_{\gamma 0}^2} \tag{16}$$

or alternatively, in order for the beam waist to fall inside the undulator one needs to satisfy a condition on the modulation (chirp rate) coefficient:

$$S = \frac{c\gamma_0\left(1+\sqrt{1-\frac{4R_{56}^2\sigma_{\gamma 0}^2}{c^2\gamma_0^2\sigma_{t0}^2}}\right)}{2R_{56}} \approx \frac{c\gamma_0}{R_{56}} \tag{17}$$

At the waist, the ellipse is erect:

$$\phi_w(L_w,\gamma,t) = \frac{(\Delta t)^2}{2\sigma_{tw}^2} + \frac{(\Delta\gamma)^2}{2\sigma_{\gamma w}^2} \tag{18}$$

where σ_{tw} is the bunch duration at waist and $\sigma_{\gamma w}$ is the energy spread at waist.

Substituting (17) or (16) in (15), the radii of the erect ellipse are found to be:

$$\frac{1}{\sigma_{tw}^2} = \frac{1}{\sigma_{t0}^2} + \frac{S^2}{\sigma_{\gamma 0}^2} \tag{19}$$

$$\frac{1}{\sigma_{\gamma w}^2} = \frac{1}{\sigma_{\gamma 0}^2} + \frac{R_{56}^2}{c^2\gamma_0^2\sigma_{t0}^2} + \frac{S^2R_{56}^2}{c^2\gamma_0^2\sigma_{\gamma 0}^2} - \frac{2R_{56}|S|}{c\gamma_0\sigma_{\gamma 0}^2} \tag{20}$$

Since we expect compression - $\sigma_{tw} \ll \sigma_{t0}$, we can approximate Eq. (19) a to:

$$\sigma_{tw} \approx \frac{\sigma_{\gamma 0}}{S} \tag{21}$$

We conclude that the bunch duration at the waist is limited by the intrinsic energy spread (defined as the uncorrelated beam energy spread at its waist before modulation).

Note that in the framework of the linear model, the phase space area is conserved throughout the beam transport from the gun to the wiggler, $\sigma_{t0}\sigma_{\gamma 0} = \sigma_{tw}\sigma_{\gamma w}$, as can be confirmed by substitution of equation 20, 19, or 21 and 17.

5 Bunch transport and compression in the configuration of the ORGAD accelerator

We follow the phase space evolution of the beam for the example of the ORGAD accelerator using the linear transformation phase-space model. Bear in mind that this model is limited, does not include space-charge effects and nonlinear phase space evolution. Also, it is assumed that the amplitude of the superradiant radiation field is low (below saturation), and the beam dynamics is independent of the emitted radiation, namely, the emitted radiation does not act back on the particles. Therefore the linear model can serve only as a preliminary guide for the design of the superradiant FEL, and further on it should be checked and compared to the results of detailed GPT transport simulations that include consideration of space-charge effects. Such simulations are shown in Supplementary Appendix A for the ORGAD parameters where the beam transport was adjusted to produce a ribbon beam in the undulator in order to reduce space-charge effects.

We calculate the compaction factor from the end of the gun to the center of the undulator. This is given as a sum of the free drift compaction factor from the gun to the undulator and the compaction factor of half the length of the undulator $R_{56}^{(a)}+R_{56}^{(b)} = R_{56}$. As derived in Supplementary Appendix C, for $\gamma_0 = 13.1$ and $L_e = 3.24$[m] (L_e is the drift length from the gun ($z = 0$) to the entrance of the undulator), $R_{56}^{(a)} = \frac{L_e}{\gamma_0^2} = 1.89[cm]$, $R_{56}^{(b)} = 0.33$ [cm] for half of the undulator length $z_{hw} = \frac{L_w}{2} = 40[cm]$, and $a_w = 0.915$. Finally, the compaction factor from the end of the gun to the center of the undulator is $R_{56}^{(a)}+R_{56}^{(b)} = R_{56} = 2.22$[cm].

For these parameters we calculate the modulation coefficient desired for attaining a waist at the center of the undulator. The starting parameters for the linear phase-space evolution are taken from the GPT simulation of the gun section (see Supplementary Appendix A): the intrinsic energy spread is $\sigma_{\gamma 0} = 0.01$ ($\sigma_{E0} = 5$ keV), and the beam bunch size at the gun is $\sigma_{t0} = 1$[ps]. Using Eq. (17), this results in $S = 1.77*10^{11}$[1/sec], which is fairly consistent with the computed chirp rate shown in the last panel of Supplementary Appendix Figure SA1. According to eq. 21 and eq. (20), these parameters should enable attaining a beam waist of $\sigma_{tw} \approx 60$ [fs] at the center of the undulator length with $\sigma_{\gamma w} = 0.12$.

This result of an ideal linear transport model is an underestimate relative to the result of a full GPT simulations with the parameters of the ORGAD hybrid photocathode gun. The GPT simulation along the entire beam transport results in a beam bunch waist $\sigma_{tw} = 70$[fs] at the center of the undulator (see lower part of Figure 1 and Supplementary Appendix A). This is slightly bigger than the estimate of the linear model.

In order to compare the beam size evolution in the linear phase space model to the numerical GPT simulation we trace back the phase-space ellipse evolution from the waist location at the center of the undulator backward.

We start from Eq. 14 and assume that the phase-space ellipse is erect at the waist point in the middle of the undulator $z = L_0$, evolves with z (within and before the undulator) according to:

$$\phi(\gamma,t,z) = \frac{\left(t - t_0 + \frac{R_{56}(L_0)-R_{56}(z)}{c}\frac{\gamma-\gamma_0}{\gamma_0}\right)^2}{2\sigma_{tw}^2} + \frac{(\gamma-\gamma_0)^2}{2\sigma_{\gamma w}^2} = 1 \tag{22}$$

The compaction factor dependence on z starting from the exit of the gun $z = 0$ is (Supplementary Appendix C):

$$R_{56}(z) = \frac{1}{\gamma_0^2}\left(z\frac{a_w^2}{2}(z-L_e)\eta(z-L_e)\right) \tag{23}$$

where η is the step function, and $L_0 = L_e + L_w/2$.

From here we derive the size of the beam (the projection of the ellipse on the time axis t [7]:

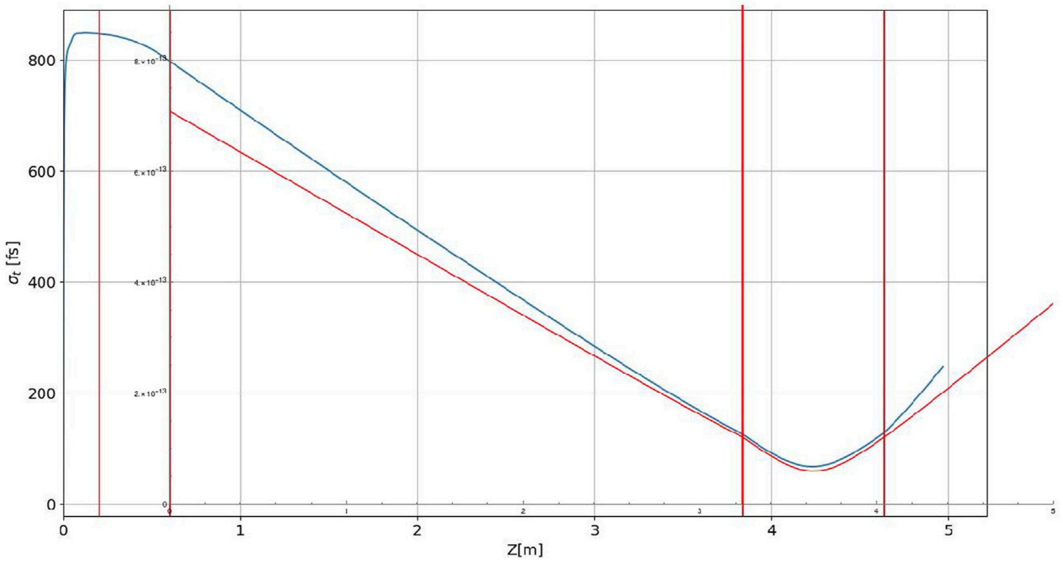

FIGURE 7
Plot of the bunch size evolution $\sigma_t(z)$ traced back to the gun exit from the waist position at the center of the undulator using Eq. 24 (see red curve). GPT simulation plot of the bunch size evolution from the gun cathode and beyond the undulator (blue curve), is overlayed over the analytical calculation plot. The first vertical red lines mark the acceleration and chirping sections of the gun, the last two red lines mark the undulator section.

$$\sigma_t(z) = \sigma_{tw}\left[1 + \left(\frac{R_{56}(L_0) - R_{56}(z)}{c\gamma_0}\right)^2 \frac{\sigma_{\gamma w}^2}{\sigma_{tw}^2}\right]^{\frac{1}{2}} \tag{24}$$

This curve is shown in Figure 7 for the earlier computed parameters $\sigma_{tw} \approx 60$ [fs], $\sigma_{\gamma w} = 0.12$.

In Figure 7 we also show the corresponding results of GPT simulations for the same parameters overlayed over the same coordinate axis. The simulated curve deviates approximately by 20% at the start of the drift section (exit of the gun). The discrepancy is attributed to space charge expansion of the bunch along the drift section and in the undulator.

6 Conclusion

Bunched beam superradiance is an attractive concept for attaining intense THz radiation in a compact FEL scheme [1, 3, 14–16]. Here we presented theory and design consideration of a superradiant waveguide FEL based on a compact (60 cm long) hybrid photocathode RF gun. For the configuration of the ORGAD accelerator, an 80 cm long undulator and a modest beam bunch charge of 20 pC, we predict for an ideally short bunch, emission of about W = 60 nJ radiation at the fundamental transverse radiation mode LSM01 at frequency 3.4 THz and nearly 1 μJ in 9 transverse modes in the frequency range 2.5–3.5 THz. To attain these energies, one is required to attain compression of the beam to short duration - $\sigma_t < 1/2\pi f$. For a nonoptimized design based on the ORGAD accelerator parameters and GPT simulations, including space-charge effects, a bunch duration of $\sigma_t = 70\, ftS$ was calculated, which corresponds to reduction of the radiation emission by a bunching factor of 0.1 to 0.3 for the different modes. In the presented design the bunch duration was limited by space charge effects in the undulator section. It may be possible to mitigate these space-charge effects by proper shaping of the beam transverse and longitudinal profiles at the gun and at the entrance to the undulator [14] and thus restore the emission energies predicted for an ideal beam.

It is instructive to compare the parameters of the superradiant THz FEL design to the alternative scheme of enhancing spontaneous undulator radiation by SASE [17]. The superradiance enhancement factor relative to spontaneous emission is N = Q/e, the number of electrons in the beam. This factor is 10^8 for Q = 20 pC. Larger enhancement factors are attainable by the SASE scheme, but this requires much longer undulator, higher beam energy and higher beam charge [17, 18]. In PITZ the measured terahertz energy was two orders of magnitude (tens of μJ) higher in the same spectral range. However, this required threefold larger beam energy, fourfold longer undulator and two orders of magnitude higher charge. The bandwidth of an isolated single mode of the superradiant FEL design example is 2.5%, comparable to the SASE spectrum, but if one considers the multimode spectrum shown in Figure 3, it lies in the wide range 2.8–3.5 THz. For many applications of diagnostics and radiation effect research, particularly in university laboratories, only moderate radiation energy is required and accelerator dimensions and costs matter. For such applications, superradiant FEL may have an advantage.

We presented an analytical model evaluation for the evaluation of superradiannt energy and spectral distribution [1, 3], and compared the results to numerical computations using UCLA GPTFEL code. We found fair agreement between the radiation spectrum and the integrated radiation energy per mode computed using the code and using the analytical expression.

We presented a linear model for tracing the beam compression dynamics in energy-time phase-space evolution from the electron gun through free drift up to and within the undulator. This model is a useful tool for preliminary design of a superradiant FEL, however, it has limited validity because it does not take into consideration space-charge effects and nonlinear distortion of phase-space trajectories transformation. The model helped to recognize that the attainment of short bunches in the undulator and high frequency operation is limited also by the intrinsic (uncorrelated) energy spread of the gun. In realistic design, the predictions of the linear phase-space evolution model must be checked by numerical simulations that take into account apace charge effects. In the present paper we backed up the analytical model design example by GPT numerical computation that include space-charge effects. For the presented design example space charge effect deviations of the beam trajectories were moderate (20%).

Within the validity limits of the linear model, we found that the minimal temporal waist size of the beam σ_{tw} in a given beam transport configuration is given by $\sigma_{tw} \approx \frac{\sigma_{y0}}{S}$ - proportional to the intrinsic energy spread of the gun σ_{y0}. Thus, to operate the superradiant FEL at higher frequency it is necessary to minimize the intrinsic energy spread of the gun. For the example based on the ORGAD accelerator, where space charge effects are marginal, we found that a minimal bunch temporal size of $\sigma_{tw} = 70\ fs$ at the center of the undulator is attainable and is consistent with an intrinsic energy spread in the gun of $\sigma_{E0} = 5$ keV. This is quite consistent with the GPT simulation results of the Gun (Supplementary Appendix Figure SA1). Deviation may be expected also because of the neglect of nonlinear effects in the phase-space evolution along the transport line that are not taken into account in the linear phase space model. These values of the intrinsic energy spread in the gun are similar to measurements of uncorrelated energy spread of photocathode RF-gun injectors in other laboratories [19]. Measurements at SwissFEL 110 m distance from the rf gun showed 15 keV for 200pC, and 6.5 keV for 10pC, while the simulation results predict well below 1 keV [20]. The discrepancy between the measurement and simulations is related to IBS (Intrabeam scattering) and MBI (microbunching instability) between the gun and the measurement point. Measurements at European XFEL, 40 m from the gun area, for beam charge of 250 pC show slice energy spread of 6 keV [21]. More recent publications reported slice energy spread of 2 KeV for 250pC, 20 m from the rf gun at the PhotoInjector Test facility at DESY Zeuthen (PITZ) [22].

The bunch duration in the ORGAD Accelerator design is also bound by the energy spread of the photocathode gun. GPT simulations in the gun section indicate intrinsic energy spread in the gun of ~5 keV for a beam of charge of 20 pC that should be attributed to space charge effects in the early acceleration stages in the gun. We conclude that for the design example parameters, both the intrinsic energy of the gun (due to space charge effects) and space charge effects in the undulator limit the attainment of beam compression below $\sigma_{tw} \approx 70\ ftS$ and consequently the bunching factor (Eq. (7)) would diminish the superradiant radiation at frequencies beyond 3 THz. Attainment of higher frequency superradiance in future superradiant FEL designs requires technological advance in reduction of the intrinsic energy spread of the gun or enhancement of the modulation (chirp) factor S, (that would require also a shorter drift length to the undulator) and mitigation of space charge effects in the undulator region, possibly by optimizing the dimensions and distribution shape of the beam [14].

Data availability statement

The original contributions presented in the study are included in the article/Supplementary Material, further inquiries can be directed to the corresponding author.

Author contributions

AW: Investigation, Writing–original draft. AG: Supervision, Writing–original draft. AN: Supervision, Writing–review and editing. AhF: Methodology, Writing–review and editing. RI: Validation, Writing–review and editing. AnF: Software, Writing–review and editing. PM: Methodology, Software, Writing–review and editing. AtF: Writing–review and editing. JR: Methodology, Writing–review and editing.

Funding

The author(s) declare financial support was received for the research, authorship, and/or publication of this article. We acknowledge support by the Israel Science Foundation through grant 1705/22.

Conflict of interest

The authors declare that the research was conducted in the absence of any commercial or financial relationships that could be construed as a potential conflict of interest.

Supplementary material

The Supplementary Material for this article can be found online at: https://www.frontiersin.org/articles/10.3389/fphy.2024.1385314/full#supplementary-material

References

1. Gover A, Ianconsescu R, Friedman A, Emma C, Sudar N, Musumeci P, et al. Superradiant and stimulated-superradiant emission of bunched electron beams. *Rev Mod Phys.* (2019) 91:035003. doi:10.1103/revmodphys.91.035003

2. Dicke RH. Coherence in spontaneous radiation processes. *Phys Rev* (1954) 93(99): 99–110. doi:10.1103/physrev.93.99

3. Gover A. Superradiant and stimulated-superradiant emission in prebunched electron-beam radiators. I. Formulation. *Phys Rev St-accl Beams* (2005) 8:030701. doi:10.1103/physrevstab.8.030701

4. Nause A, Friedman A, Weinberg A, Borodin D, Feigin L, Fukasawa A, et al. 6 MeV novel hybrid (standing wave - traveling wave) photo-cathode electron gun for a THz superradiant FEL. *NIM-A* (2021) 1010. doi:10.1016/j.nima.2021.165547

5. Ferrario M, Alesini D, Bacci A, Bellaveglia M, Boni R, Boscolo M, et al. Experimental demonstration of emittance compensation with velocity bunching. *Phys Rev Lett* (2010) 104(5):054801. doi:10.1103/physrevlett.104.054801

6. Anderson S, Musumeci P, Rosenzweig JB, Brown WJ, England RJ, Ferrario M, et al. Velocity bunching of high-brightness electron beams. *Phys Rev St-accel Beams* (2005) 8(1):014401. doi:10.1103/physrevstab.8.014401

7. Rosenzweig JB. *Fundamentals of beam Physics*. Oxford: Oxford Universty Press (2003).

8. Weinberg A, Nause A. Dogleg design for an MeV ultra-fast electron diffraction beamline for the hybrid photo-emitted RF GUN at ariel university. *NIM-A* (2021) 989. doi:10.1016/j.nima.2020.164952

9. Weinberg A, Nause A. Beam-line optimization based on realistic electron-optics 3D field-maps implementation provides high-quality e-beam via a dogleg section. *Phys Plasmas* (2022) 29. doi:10.1063/5.0087858

10. Jerby E, Gover A. Investigation of the gain regimes and gain parameters of the free electron laser dispersion equation. *IEEE J Quan Electron* (1985) 21(7):1041–58. doi:10.1109/jqe.1985.1072748

11. Zhang k., Li D. *Electromagnetic theory for microwaves and optoelectronics*. Springer (2013).

12. Fisher A, Musumeci P, Van der Geer S. Self-consistent numerical approach to track particles in free electron laser interaction with electromagnetic field modes. *Phys Rev Acc ad Beams* (2020) 23(11):110702. doi:10.1103/physrevaccelbeams.23.110702

13. Musumeci P, Fisher A, Van Der Geer B, Nanni EA, Snively EC, Gover A. A Waveguide-Based High efficiency superradiant FEL operating in the THz regime. In: FEL2019*, hamburg* (2019).

14. Siriwan K, Shuya C, Heishun Z, Toshiteru K, Hideaki O. Manipulation of laser distribution to mitigate the space-charge effect for improving the performance of a THz coherent undulator radiation source. *particles MDPI* (2018) 1(1):238–52. doi:10.3390/particles1010018

15. Siriwn K, Heishun Z, Shuya C, Toshiteru K, Hideaki O. Properties of THz coherent undulator radiation generated from a compact accelerator source at Kyoto University. *Rev Sci Inst* (2019) 90(10):103307. doi:10.1063/1.5110342

16. Joshi V, Karmakar J, Kumar N, Karmakar B. Theoretical and simulation study of ′comb′ electron beam and THz generation (2018). Available from: https://arxiv.org/abs/1806.04338 (Accessed 12 June 2018).

17. Krasilnikov M, Aboulbanine Z, Asoyan A, Davtyan H, Boonpornprasert P, R G. First lasing of the THz SASE FEL at PITZ. In: *FEL22, trieste* (2022).

18. Krasilnikov M, Aboulbanine Z, Adhikari G, Aftab N, Asoyan A, Davtyan H. THz SASE FEL AT PITZ: LASING AT A WAVELENGTH OF 100μm. In: *IPAC, venice* (2023).

19. Prat E, Lucas TG, Dijkstal P, Di Mitri S, Ferrari E, et al. Energy spread blowup by intrabeam scattering and microbunching at the SwissFEL injector. *Phys Rev Accel Beams* (2022) 25(10):104401. doi:10.1103/physrevaccelbeams.25.104401

20. Prat E, Dijkstal P, Ferrari E, Malyzhenkov A, Reiche S. High-resolution dispersion-based measurement of the electron beam energy spread. *Phys Rev Accel Beams* (2020) 23:090701. doi:10.1103/physrevaccelbeams.23.090701

21. Tomin S, Zagorodnov I, Decking W, Golubeva N, Scholz M. Accurate measurement of uncorrelated energy spread in electron beam. *Phys Rev Accel Beams* (2021) 24(6):064201. doi:10.1103/physrevaccelbeams.24.064201

22. Qian H, Krasilnikov M, Lueangaramwong A, Li X, Lishilin O, Aboulbanine Z, et al. Slice energy spread measurement in the low energy photoinjector. *Phys Rev Accel Beams* (2022) 25(8):083401. doi:10.1103/physrevaccelbeams.25.083401